

Sl. No.	<p style="text-align: center;"><b>IIT Ropar</b>  <b>List of Recent Publications with Abstract</b>  <b>Coverage: November, 2023</b></p>
1.	<p><a href="#">2310P oxygen nano-bubbles attenuate hypoxia-induced tumour malignancy in tumour xenograft models</a>  <b>K Bhavya, K Agrawal, D Negi, K Niveria, AK Verma, Y Singh, NN Nirmalkar, D Pal</b> - <i>Annals of Oncology</i>, 2023</p> <p><b>Abstract</b>  Background: The rapid proliferation of cancer cells leads to abnormal vascularization, creating a hypoxic tumor core in most advanced solid tumors. Recent studies have shown that hypoxia is associated with poor prognosis in cancer patients. Tumor aggressiveness is driven by hypoxia, which confers resistance to many conventional cancer therapies. In the present study, we propose that oxygen nanobubbles can reduce the hypoxic effect on the epithelial-to-mesenchymal transition (EMT) and prevent migration and invasion in non-small cell lung cancer (NSCLC) and triplenegative breast cancer (TNBC).  Methods: Using the sonic cavitation method, we have developed a method to generate bulk oxygen nanobubbles (ONBs) with dipalmitoyl phosphatidylcholine (DPPC) lipid and quantitate mean diameter and number density through nanoparticle tracking analysis and insight. We have treated A549 lung adenocarcinoma and MDAMB-231 triple-negative breast cancer cell lines with 1% oxygen and ONB. We have also checked its preventive role in the zebrafish tumor xenograft model. We have measured HIF-1a and EMT expression markers by immunoblot and qPCR analysis. Moreover, we have used the 4T1 BALB/c mice tumor xenograft model for further confirmation.  Results: ONB promotes HIF-1a hydroxylation and its proteasomal degradation in hypoxic cancer cells. ONBs treated A549 and MDA-MB-231 cancer cells and an adult zebrafish A549 tumor xenografts showed the downregulation of TGF-<math>\beta</math> and VEGFA expression at the transcriptional and translational levels, which also led to upregulation of epithelial genes like E-cadherin with down-regulation of mesenchymal genes like N cadherin, Vimentin, Fibronectin. ONB treatment significantly affects cancer cell migration. Also, liposomal ONB administrated 4T1 BALB/c breast tumor xenograft model showed similar results.  Conclusions: ONBs reduce HIF-1 mediated epithelial to mesenchymal transition (EMT) controlled by TGF-<math>\beta</math> and VEGFA and prevent cellular migration and invasion in solid tumors, particularly NSCLC and TNBC. In conclusion, targeted administration of ONB could be a better therapeutic approach to inhibit the hypoxic detrimental effect, which helps to increase the efficacy of anticancer treatments.</p>
2.	<p><a href="#">A deep learning approach for early detection of drought stress in maize using proximal scale digital images</a>  <b>P Goyal, R Sharda, M Saini...</b> - <i>Neural Computing and Applications</i>, 2023</p> <p><b>Abstract:</b>  Neural computing methods pose an edge over conventional methods for drought stress identification because of their ease of implementation, accuracy, non-invasive approach, cost-effectiveness, and ability to predict in real time. To ensure proper irrigation scheduling and prevent major yield losses, the objective was to develop a deep learning (DL)-based custom convolutional neural network (CNN) framework for in situ identification and classification of drought stress in maize crops. An original image dataset was created by acquiring 2703 RGB images of maize crops under natural daylight conditions to incorporate noise and varied backgrounds. The dataset was augmented and divided in a ratio of 7:2:1 for the training, validation, and test sets. A custom-CNN model was built using feature blocks, fully connected layers, and dense layers, and compared with five state-of-the-art CNN architectures, i.e.</p>

	<p>InceptionV3, Xception, ResNet50, DenseNet121 and EfficientNetB1. The results revealed that the custom CNN model achieved accuracies of 98.71% and 98.53% on the training and test sets, respectively. In comparison, the ResNet50 and EfficientNetB1 transfer-learned CNN architectures achieved an equivalent accuracy of 99.26% each, followed by DenseNet121 with a 98.90% accuracy on the test set. The Xception model performed the worst, with the highest accuracy of 91.91% on the test set. The results demonstrate that the developed custom CNN model should be adopted for real-time implementation on resource-constrained edge devices because of the lower number of parameters (0.65 million parameters) compared to other state-of-the-art architectures.</p>
3.	<p><a href="#">A perspective on the future of electrochemical ammonia synthesis: aqueous or non-aqueous?</a>  <b>D Gupta, A Kafle, S Kaur, TC Nagaiah - Journal of Materials Chemistry A, 2023</b></p> <p><b>Abstract</b></p> <p>Ammonia (NH<sub>3</sub>) production is deemed to address the hunger issues of the drastically mounting population due to its huge significance in the fertilizer industry. The quest is ongoing to reduce the CO<sub>2</sub> emissions and energy consumption by traditional Haber-Bosch process for bulk ammonia production in industries. The most promising alternative to the same is electrochemical ammonia production, which leads to zero carbon emission, can be operated under mild conditions, and is energy efficient. Unfortunately, the faradaic efficiency (FE) and ammonia yield rate are far below the practical standards, and only a few breakthrough works are available in the literature with more than 50% FE. In past years, the majority of the research has grown in view of the development of electrocatalysts to enhance the FE and yield rates. Although the design of the electrode is crucial to determine the performance of the overall process, the effect of electrolyte and synergy between electrolyte and electrode is equally important but underexplored. So, in this perspective, we summarize the breakthrough works in electrochemical ammonia production under both aqueous and non-aqueous environments. Besides, different strategies and modifications in electrolytes, electrode-electrolyte interface have been discussed that may lead to a decisive interpretation of “the actual future of ammonia production, i.e., either aqueous or non-aqueous?” based on their existing challenges and future potential for real-time application and industrialization. In the end, the overall outlook and future opportunities in this regard have been proposed, deliberating a stern remark on the underlooked aspects in this field. This perspective will open a floor for further investigations and improvements in aqueous and non-aqueous ammonia production capable of meeting the practical standards and a green revolution.</p>
4.	<p><a href="#">A planning-support tool for spatial suitability assessment of harvesting sites for stormwater infrastructure</a>  <b>S Sharma, S Pathak, S Kumar - Journal of Hazardous, Toxic, and Radioactive Waste, 2024</b></p> <p><b>Abstract</b></p> <p>Increasing water shortages and the effects of global climate change require us to adopt sustainable methods to protect our natural water sources. Of all the techniques that are used to conserve water, stormwater harvesting (SWH) is considered the most sustainable approach to ease the pressure on freshwater resources. It is difficult to use multicriteria methods to estimate the potential of stormwater and identify appropriate locations for SWH. Therefore, this study proposes a robust method for assessing the potential of SWH and finding appropriate sites, which consider the suitable criteria for site selection. A geographic information system (GIS)-based approach is used to screen and identify areas with high potential for SWH, followed by a detailed analysis. Subsequently, to evaluate and analyze SWH sites, multiple suitability criteria are established with input from water experts to aid in the decision-making. The first step involves shortlisting potential sites and identifying suitable locations within the subcatchments. Thematic layers are created at a consistent spatial scale and used as input data for the model. The GIS environment is utilized to conduct computations that use the distributed curve number (CN) method, which helps when estimating the spatial distribution of event-based runoffs. Following</p>

	<p>the establishment of the thematic layers, an analytical hierarchy process (AHP) is employed to allocate proportional importance to each layer. This culminates in the production of a suitability map for SWH within the designated study region. The study could benefit water planners, because it enables them to identify suitable locations and make informed decisions at a regional scale.</p>
5.	<p><a href="#">A review on environmental concerns and technological innovations for the valorization of steel industry slag</a>  <b>SS Chandel, PK Singh, PK Katiyar...</b> - Mining, Metallurgy and Exploration, 2023</p> <p><b>Abstract</b>  Mineral process wastes, such as metallurgical slags nowadays, are of significant metals and materials resources in the circular economy. The usability of iron-making slag is well established; however, steel slag still needs to be utilized due to various physicochemical constraints. In this context, we have reviewed the global steel slag generation, processing, characteristics, and potential application with suggestions for futuristic possibilities to address the technical, economic, and environmental aspects of steel slag recycling. The steel slags inherit characteristics from ore chemistry and their processing routes, which may be Blast Furnace-Basic Oxygen Furnace (BF-BOF) or Direct Reduced Iron-Electric Arc Furnace (DRI-EAF) steel-making routes with/without treatment in a Ladle Furnace (LF). The average generation of slags in BOF, EAF, and LF processes accounts for 110 kg, 70 kg, and 40 kg per tonne of steel, respectively. Considering global steel production of 1878 million tonnes in 2020, the associated slag by-products possess a significant resource of major components like FeO, CaO, SiO<sub>2</sub>, Al<sub>2</sub>O<sub>3</sub>, etc. Selecting a recycling technique depends on the slag's end use, logistics, and physicochemical characteristics. BOF and EAF slag are used ~ 48% in road construction applications and ~ 10% for industrial specific metallurgical use. EAF slag is preferred as cementitious material as compared to BOF. Hot-stage modification of BOF slag has emerged as a preferred method to achieve desired chemical and subsequent mechanical properties for end use. BOF slag has high carbon dioxide sequestration potential for in-plant remediation among steel slags.</p> <p><b>Author keywords</b>  Circular economy; Mineral processing waste; Recycling; Resource recovery; Steel slag</p>
6.	<p><a href="#">Algorithms and hardness results for edge total domination problem in graphs</a>  <b>MA Henning, A Pandey, G Sharma, V Tripathi</b> - Theoretical Computer Science, 2023</p> <p><b>Abstract</b>  For a graph <math>G=(V,E)</math> without an isolated edge, a set <math>D \subseteq E</math> is an edge total dominating set of <math>G</math> if every edge <math>e \in E</math> is adjacent to at least one edge of <math>D</math>. The MINIMUM EDGE TOTAL DOMINATING SET problem is to compute a minimum cardinality edge total dominating set of <math>G</math>. It is known that the decision version of the problem is NP-complete for bipartite graphs, chordal graphs, and planar graphs. On the positive side, the problem is efficiently solvable for trees. In this paper, we further study the complexity of this problem in other graph classes. We design a linear-time algorithm to compute a minimum cardinality edge total dominating set in chain graphs, a subclass of bipartite graphs. We also propose linear-time algorithms for two subclasses of chordal graphs, namely, split graphs and proper interval graphs with no cut vertices. In addition, we show that the problem is APX-complete for graphs with maximum degree 3 and propose an approximation algorithm for the problem in <math>k</math>-regular graphs, where <math>k \geq 4</math>. We discuss the complexity difference between the MINIMUM EDGE DOMINATING SET problem and MINIMUM EDGE TOTAL DOMINATING SET problem which seem to be closely related.</p>
7.	<p><a href="#">Analysing mismatch effect of CMOS neurons in spiking neural network with winner-take-all mechanism</a>  <b>SK Vohra, AP James, M Sakare, DM Das</b> - 2023 IEEE Nordic Circuits and Systems</p>

	<p>Conference (NorCAS), 2023</p> <p><b>Abstract</b></p> <p>The aim of designing the energy-efficient high-density spiking neural network (SNN) is not possible without channelising the efforts to design the basic repeating blocks of Neuromorphic Computing (NMC), i.e., neurons and synapses. The investigation done to replace synapses in the last years has created memristors as the most prominent solution for high-density SNN. CMOS-memristive integrated circuits are widely adopted to realise brain-inspired neuromorphic circuits. While the challenges of the memristors have been highlighted and resolved in various literature, much attention is not given to designing robust CMOS neurons and its challenges for achieving high-density integration in neuromorphic chips. Process-induced variations must be analysed for the robustness of the CMOS neurons. Apart from the process and temperature variations of CMOS neuron, which is mostly analysed in previous works, mismatches are critical for the SNN with a winner-take-all (WTA) mechanism where output neurons compete to win the competition. In this paper, we have shown that the SNN with WTA mechanism is robust to PVT variations but is sensitive to mismatch variations of CMOS neurons. We have also proposed an approach to mitigate the mismatch effect. The observations are validated with the post-layout simulation results of the SNN circuit designed in 180 nm CMOS technology.</p>
8.	<p><a href="#">Analytical and numerical models of a new hybrid system of earth air tunnel integrated solar air heater with sensible storage</a>  S Verma, R Das - Journal of Solar Energy Engineering, 2023</p> <p><b>Abstract</b></p> <p>A novel combination of an earth air tunnel (EAT) and a sensible thermal storage-aided solar air heater has been proposed when the sensible storage medium is taken to be rocks filled within the air flow passage. Both transient and steady state models are presented. The former describes exact thermal behaviour of the system for a two-month winter period for the city of Baghdad, Iraq. The latter describes average performance of the system. The implicit finite difference method and method of separation of variables have been used to solve the pertinent equations in the respective models. Acceptable level of accuracy was obtained between the steady-state numerical and analytical solutions as well as between the numerical and the published data. It is revealed that preheating by a sufficiently long EAT module improves the effective power as well as the output temperature from the rock bed solar air heater by about 35% and 9% respectively for the present set of parameters considered. It is also observed that for the present set of parameters considered, the temperature gradients in the direction normal to air flow in the solar air heater are insignificant and may be ignored. A parametric study is also presented that assesses the impact of system parameters on the quality as well as quantity of the energy extracted from the system. This work is hence the first to couple an EAT with a sensible thermal storage equipped solar air heater and may pave way for future studies.</p> <p><b>Keywords</b>  geothermal, heating, solar, Storage, system</p>
9.	<p><a href="#">Antenna gain and factor extraction of EMC test antennas by two- and three-antenna measurement methods in a comparative manner</a>  G Köse, LK Baghel, Y Soylu, SA Sis, C Coşar, S Kumar - International Electromagnetic Compatibility Conference (EMC Türkiye), 2023</p> <p><b>Abstract</b></p> <p>The two and three-antenna measurement methods are well-known techniques for characterizing the antenna gain and antenna factor and are often utilized for calibrating the test antennas. This paper presents the antenna gain and antenna factor extractions of horn-type EMC test antennas from both two and three-antenna measurement results. Three same-type horn antennas, operating</p>

	<p>up to 18 GHz, are measured in three different combinations as pairs. The antenna gains and antenna factors are first extracted from each pair (two-antenna) measurements separately and then also extracted simultaneously from all three measurement combinations (three-antenna). Extracted results show that the antenna's identicalness is a necessity to achieve accurate results in two-antenna measurement results, while the three-antenna method does not rely on the identicalness of the three antennas.</p>
10.	<p><a href="#">Assessment of changes in monthly streamflow using innovative polygon trend analysis in the South Indian Rivers</a>  <b>N Gupta, SR Chavan</b> - Arabian Journal of Geosciences, 2023</p> <p><b>Abstract</b>  This study focuses on a hydro-meteorological variable, streamflow, and its vulnerability to global warming. In this study, we analyze monthly streamflow in 40 catchments across four major South Indian River basins: Cauvery, Godavari, Krishna, and Mahanadi, within the Indian Peninsular region. The chosen catchments have available streamflow series records ranging from 41 to 49 years, spanning from 1970 to 2018. To uncover trends in the streamflow datasets, an innovative technique called Innovative Polygon Trend Analysis (IPTA) is used. IPTA detects trend transitions between successive time series parts and identifies possible trend pieces within a year, crucial for agricultural and irrigation practices. Results reveal diverse polygon patterns across different catchments, reflecting non-systematic streamflow variation. Non-systematic changes occur primarily in the Cauvery basin, followed by the Godavari, Krishna, and Mahanadi basins. Varied trends—increasing and decreasing—are dispersed across different catchments. Increasing trends were generally observed in the standard deviation of streamflow, while decreasing trends were more widespread in the mean of streamflow. Notably, the Godavari basin displays more prevalent decreasing trends in the majority of catchments for different months, followed by Cauvery and Krishna. Mahanadi basin has more catchments showing an increasing trend than other basins. The results of this study provide deeper insight into the streamflow dynamics within these four basins.</p>
11.	<p><a href="#">BEAMER: Behavioral encoder to generate multiple appropriate facial reactions</a>  <b>X Hoque, A Mann, G Sharma, A Dhall</b> - Proceedings of the 31st ACM International Conference on Multimedia, 2023</p> <p><b>Abstract</b>  This paper presents a framework for generating appropriate facial expressions for a listener engaged in a dyadic conversation. The ability to produce contextually suitable facial gestures in response to user interactions may enhance the user experience for avatars and social robots interaction. We propose a Transformer and Siamese architecture-based approach for generating appropriate facial expressions. Positive and negative Speaker-Listener pairs are created, applying a contrastive loss to facilitate learning. Furthermore, an ensemble of reconstruction quality sensitive loss functions is added to the network for learning discriminative features. The listener's facial reactions are represented with a combination of the 3D Morphable Model's coefficients and affect-related attributes (facial action units). The inputs to the network are pre-trained Transformer-based feature MARLIN and affect-related features. Experimental analysis demonstrate the effectiveness of the proposed method across various metrics in the form of an increase in performance compared to a variational auto-encoder-based baseline.</p>
12.	<p><a href="#">Biodiversity sensor: A customized and power efficient solution for biodiversity surveillance</a>  <b>M Kaur, K Singh, S Kumar</b> - IEEE Sensors Journal, 2023</p> <p><b>Abstract</b>  Pollinators play a vital role in ecosystem conservation, and their extinction would pose a serious threat to our existence. Recent research has revealed that excessive use of pesticides, fertilizers and changing farming practices has adversely affected pollinator biodiversity. Therefore,</p>



	<p>continuous farmland monitoring is required to check flying insects for biodiversity conservation. The idea is to develop a digital sensor network across farmlands for the monitoring of biodiversity at a large scale. In this paper, a Biodiversity Sensor (BS) is developed that can track the movement of flying insects in real-time, along with environmental conditions and updates to the cloud server. The developed sensor is a processor-based IoT device, powered by a solar-PV/battery bank and loaded with a customized Linux operating system (using Yocto-build). An over-the-air (OTA) update feature has been added to the customized OS, allowing remote management and sensor updates that were previously unavailable in the pre-installed multimedia Operating System (OS). The sensor can also be managed locally using the Device Manager Portal (DMP), which exposes sensor configuration and data download features over a local Wi-Fi hotspot. The developed sensor has been tested in the field, and the result shows that the BS effectively captures the frames of flying insects and performs surveillance appropriately with an accuracy of more than 90%. A comparison of power efficiency and CPU utilization is also made between the pre-installed multimedia OS from the manufacturer and the customized OS built using Yocto-build. Results demonstrate that the developed BS is power efficient.</p>
13.	<p><a href="#">C(sp<sup>3</sup>)–C(sp<sup>3</sup>) radical-cross-coupling reaction via photoexcitation</a>  <b>S Patel, A Chakraborty, I Chatterjee</b> - Organic Letters, 2023</p> <p><b>Abstract</b>  The photoexcitation of 4-alkyl-1,4-dihydropyridines (alkyl-DHPs) in the presence of a base triggers the single-electron-transfer-mediated desulfonative radical-cross-coupling (RCC) reaction without the need for any metal or photocatalyst. 4-Alkyl-substituted 1,4-DHPs as the electron donor (reductant) and alkyl sulfones as the electron acceptor (oxidant) are chosen strategically as the two best-matched modular radical precursors for the construction of C(sp<sup>3</sup>)–C(sp<sup>3</sup>) bonds. Ultraviolet light-emitting diodes (365 nm) have proven to be adequate for inducing single-electron transfer between two radical precursors in the excited state. Following this designed strategy, a diverse collection of primary, secondary, and tertiary persistent alkyl radicals from both radical precursors have been used to forge C(sp<sup>3</sup>)–C(sp<sup>3</sup>) bonds. This blueprint features good functional group compatibility, a broad scope, and detailed mechanistic investigation.</p>
14.	<p><a href="#">Crack driving forces under creep conditions in presence of material inhomogeneity</a>  <b>A Tiwari, AK Mishra</b> - Materials at High Temperatures, 2023</p> <p><b>Abstract</b>  Under time-dependent creep deformation in metallic materials in the presence of a crack, the driving force is influenced at a distance in the presence of a zone (such as an interlayer, interface, hole, etc.) which deforms differently in reference configuration. This influence may increase or decrease the crack driving force based on the type of inhomogeneity (elastic, plastic, creep). The nature and extent of influence of material inhomogeneity are studied in this work with a configurational force-based rate of crack driving force definition for a crack in the presence of dissimilar metal weld zone, HAZ and second base metal.</p>
15.	<p><a href="#">Crosstalk reduction in coupled microstrip lines using interdigital split on reference plane</a>  <b>LK Baghel, S Kumar, SA Sis</b> - 7th International Electromagnetic Compatibility Conference (EMC Turkiye), 2023</p> <p><b>Abstract</b>  The proximity of microstrip lines in compact and dense designs leads to unwanted electromagnetic coupling, resulting in crosstalk that needs to be minimized. Various methods have been explored in the literature, including via fencing, guard trace, guard trace with via, serpentine guard trace, serpentine guard trace with vias, and serpentine microstrip lines. However, these approaches often necessitate additional spacing between the microstrip lines, difficult to fabricate, and offer limited crosstalk reduction. Hence, we propose a planar</p>

	<p>interdigital split consisting of conductive strips, arranged in a fashion similar to interdigital capacitor, and are incorporated within the space available on reference plane between the coupled microstrip lines. That is, no additional space between the lines is required for crosstalk reduction. Electromagnetic simulations are conducted using a 75x45mm RO4003 Rogers PCB within the frequency range of 1-8GHz. The results shows a significant improvement of 19dB compared to utilizing a solid ground on the reference plane. Moreover, the efficacy of the proposed interdigital split approach is reinforced by meticulous parametric analyses. These analyses can assist designers in fine-tuning the interdigital split parameters to achieve crosstalk minimization at specific frequencies.</p>
16.	<p><a href="#">Development of quadratic enhanced assumed strain elements for three-dimensional linear elasticity</a>  <b>DS Bombarde, M Agrawal, SS Gutam, A Nandy - Computers &amp; Structures, 2024</b></p> <p><b>Abstract</b>  Enhanced assumed strain (EAS) elements are widely used in the literature to address the issue of locking associated with conventional elements. However, existing literature in the context of three-dimensional (3D) elasticity problems is predominantly restricted to the eight-node linear EAS elements. Thus, existing 3D EAS elements do not exploit the superior performance offered by quadratic elements over linear elements. In the current work, we propose a novel twenty-seven node quadratic EAS element, which, to the best of our knowledge, is the first such attempt in the literature. Additionally, the manuscript also presents a six-node wedge and an eighteen-node wedge EAS element. The proposed elements are derived methodically by investigating the interrelation between the two-field Hellinger–Reissner (HR) and three-field Veubeke–Hu–Washizu (VHW) variational formulations. The robustness and performance of the proposed EAS elements is demonstrated through numerous examples.</p>
17.	<p><a href="#">Dibenzoheterole-fused s-indacenes</a>  <b>H K Saha, D Mallick, S Das - The Journal of Organic Chemistry, 2023</b></p> <p><b>Abstract:</b>  Heterole (pyrrole, thiophene, furan, thiophene-S,S-dioxide)-fused s-indacenes are known for their enhanced paratropic ring-current strength. However, the outcome of the antiaromatic properties for dibenzoheterole-fused s-indacene antiaromatics remained underexplored. Carbazole-, dibenzothiophene-, dibenzofuran-, and dibenzo[b,d]thiophene-5,5-dioxide-fused s-indacenes 1–4, respectively, were synthesized and characterized by experimental (NMR, single-crystal, UV–vis, CV) and computational (DFT) approaches to study the ground-state antiaromatic properties. Sulfone-containing 4 showed the weakest paratropic ring-current strength for the s-indacene unit, while 1–3 showed a relatively greater paratropicity for the s-indacene unit, as evidenced by the changes in <sup>1</sup>H NMR chemical shifts of s-indacene protons. Such observation was explained by the electron-withdrawing effect of the sulfone group and loss of 4n + 2 aromaticity of the heterole unit for 4 reducing its s-indacene paratropicity strength as the nonaromaticity of the heterole unit reduces the π-bond character at the dibenzo[b,d]thiophene-5,5-dioxide/s-indacene fusion site to avoid antiaromatic s-indacene ring formation. The modulation of the paratropic ring-current strength of s-indacene for 1–4 was further supported by the NICS(1)zz and ring-current (ACID) calculations.</p>
18.	<p><a href="#">Drying behaviour of nanofluid sessile droplets on self-affine vis-à-vis corrugated nanorough surfaces.</a>  <b>D Rani, S Sarkar - The European Physical journal. E, Soft Matter, 2023</b></p> <p><b>Abstract</b>  In recent years, evaporative self-assembly of sessile droplets has gained considerable attention owing to its wide applicability in many areas. While the phenomenon is well studied for smooth and isotropically rough (self-affine) surfaces, investigations comparing the outcomes on self-affine vis-à-vis corrugated surfaces remains to be done. In this experimental work, we compare the wetting and evaporation</p>

	<p>dynamics of nano-colloidal microlitre droplets on self-affine and corrugated nanorough surfaces having identical roughnesses and interface properties. The coupled influence of particle size, concentration, and surface structuring has been explored. Differences in wettability and evaporation dynamics are observed, which are explained via the interaction between wetting fluid and anisotropic surface roughness. Our findings exhibit different temporal behaviour of contact radius and angle in the evaporation process of the droplets. Further, the corrugated surface exhibits anisotropic wettability with a monotonic change in droplet shape as evaporation proceeds, finally giving rise to irregular dried patterns. The scaled rim width and crack spacing of the particulate deposits are examined. Our results can inspire fabrication of surfaces that can facilitate direction-dependent droplet motion for specific applications.</p>
19.	<p><a href="#">EDS-PhaSe: Phase segmentation and analysis from eds elemental map images using markers of elemental segregation</a>  <b>D Beniwal, V Shivam... PK Ray</b> - Metallography, Microstructure, and Analysis, 2023</p> <p><b>Abstract</b>  Scanning electron microscopy (SEM), combined with energy-dispersive spectroscopy (EDS), is an extensively used technique for in-depth microstructural analysis. Here, we present the EDS-Phase Segmentation (EDS-PhaSe) tool that enables phase segmentation and phase analysis using the EDS elemental map images. It converts the EDS map images into estimated composition maps for calculating markers of selective elemental redistribution in the scanned area and creates a phase-segmented micrograph while providing approximate fraction and composition of each identified phase. EDS-PhaSe offers two unique advantages. Firstly, it enables the direct processing of EDS elemental map images without requiring any raw or proprietary data/software, thereby allowing the analysis of EDS results available in the published literature as images. Secondly, it enables segmentation and analysis of phases even when the phase contrast is missing in backscattered micrographs, assisting in correlating the XRD and SEM-EDS data as shown in this work for a AlCoCrFeNi high-entropy alloy. © 2023, ASM International.</p> <p><b>Author keywords</b>  EDS; Elemental segregation; Energy-dispersive spectroscopy; Phase analysis; Phase segmentation</p>
20.	<p><a href="#">Effect of inelastic deformation on strain rate-dependent mechanical behaviour of human cortical bone</a>  <b>P Uniyal, S Kaur, V Dhiman, SK Bhadada, N Kumar</b> - Journal of Biomechanics, 2023</p> <p><b>Abstract</b>  In this study, the role of inelastic deformation of bone on its strain rate-dependent mechanical behaviour was investigated. For this, human cortical bone samples were cyclically loaded to accumulate inelastic strain and subsequently, mechanical response was investigated under compressive loading at different strain rates. The strain rate behaviour of fatigued samples was compared with non-loaded control samples. Furthermore, cyclic loading-induced microdamage was quantified through histological analysis. The compression test results show that the strength of fatigue-loaded bone reduced significantly at low strain rates but not at high strain rates. The difference in microcrack density was not significant between fatigued and control groups. The results indicate that the mechanism of load transfer varies between low strain rate and high strain rate regimes. The inelastic deformation mechanisms are more prominent at low strain rates but not at high strain rates. This study shed light on the role of inelastic deformation on the rate-dependent behaviour of cortical bone.</p>
21.	<p><a href="#">Effect of shapes of particle on flow and heat transfer in confined flow</a>  <b>P Suri, SA Patel</b> - Sādhanā, 2023</p> <p><b>Abstract</b>  The particles found in diverse processes such as in pneumatic conveying, food processing,</p>



	<p>drilling operations, etc., may or may not be spherical in shape. Different types of non-spherical shapes are known to play an important role in fluid–particle interactions in terms of hydrodynamics and thermal behavior. The shape effect is studied in this work for a spherical cap and circular disc having the same projected area, in cylindrical confinement of <math>\lambda</math> (<math>\equiv</math>base diameter of particle to diameter of the tube) = 0.5 for the Poiseuille flow of air (<math>Pr = 0.72</math>) over a Reynold number range <math>1 \leq Re \leq 100</math> in steady state regime. The momentum and energy equations are solved for this problem using finite element-based techniques using COMSOL Multiphysics. The obtained results for both spherical cap and circular disc are compared with a spherical shape under otherwise identical conditions. The results show that drag experienced by spherical cap is lowest in comparison to other considered shapes at low Reynolds numbers. However, this trend gets reversed at high inertial flow (<math>Re = 100</math>). Although, the heat transfer rate in the case of spherical cap is observed to be higher than that of the circular disc and sphere. Especially, at <math>Re = 1</math> rate of heat transfer from spherical cap is <math>\sim 3</math> times higher than the sphere. Furthermore, correlations have been proposed for drag coefficient and average Nusselt number over the range of Reynold number <math>1 \leq Re \leq 100</math> incorporating both the non-spherical shapes along with a sphere thereby enabling interpolation for the intermediate values in the various applications.</p>
22.	<p><a href="#">Electrocatalytic HER and magnetism performance of BiMnO<sub>3</sub> modified BaTiO<sub>3</sub> – A ultra high dielectric constant ceramic nanomaterial</a>  D Mondal, MK Adak...SP Gumfekar... - Journal of Energy Storage, 2024</p> <p><b>Abstract</b>  High dielectric constant with green hydrogen gas productivity holds promising characteristics for futuristic advanced functional materials. Ultrahigh dielectric constant covering BiMnO<sub>3</sub> modified BaTiO<sub>3</sub> (0.5BaTiO<sub>3</sub>-0.5BiMnO<sub>3</sub>, abbreviated as BTBiM5) was chemically furnished through the precursor solution decomposition method. The spherical morphological nanocrystalline ceramics contain a tetragonal phase with 32 nm crystallite size. The cationic size alteration and temperature dealing creates oxygen vacancies which are reflected in powder X-ray diffraction (XRD) pattern shifting and the presence of lower oxidation states of Bi and Mn. The BTBiM5 sintered pellet demonstrates ultrahigh dielectric constant (<math>10^8</math> order) at low frequencies (1 kHz). The relaxor-diffusive nature of BTBiM5 is identified with 1.37 diffusivity. The single semicircular Nyquist plot corresponds to non-Debye type characterizations with a grain conductivity nature. The room temperature magnetism performance finds saturation of magnetization of BTBiM5 after 200 Oe. The nanocrystalline BTBiM5 is functionalized as an electrocatalyst to produce green hydrogen gas under alkaline conditions. In this regard, 223 mV overpotential at 30 mA cm<sup>-2</sup> current density is recorded with 152 mV dec<sup>-1</sup> Tafel slope. The six-hour chronoamperometry test identifies the durability of the material during the electrocatalytic process that confers the probable grant massive footprint of such type of materials in the near future.</p>
23.	<p><a href="#">Electrochemical and spectroscopic detection of insulin using AgNPs-decorated organic derivative</a>  G Bhardwaj, R Kaur, S Saini, N Kaur, N Singh - Colloids and Surfaces A: Physicochemical and Engineering Aspects, 2023</p> <p><b>Abstract</b>  Insulin is a crucial hormone that plays a vital role in regulating blood glucose levels in the body. The accurate detection of insulin is essential for the diagnosis and management of diabetes, a chronic disease that affects millions of people worldwide. In present work, we present an approach for the detection of insulin using a 4H-chromene derivative surface decorated with AgNPs. The method involves the use of cyclic voltammetry, linear sweep voltammetry, chronoamperometry, UV–visible and fluorescence spectroscopy, all of which are carried out in an aqueous medium. Our results demonstrate that the proposed method exhibits a low detection limit of 2 nM, high sensitivity (1.77 <math>\mu\text{A nM}^{-1} \text{cm}^{-2}</math>), and excellent reproducibility (3.21 %). The electrochemical and spectroscopic measurements provide</p>

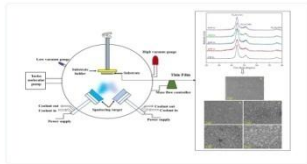
	accurate and reliable detection of insulin in various concentrations. The method's property of detecting insulin in both liquid and solid state makes it a cost-effective and environment friendly alternative to conventional detection methods, with significant implications in the field of diabetes management.
24.	<p><a href="#">Engineering the porosity and active sites in metal–organic framework</a>  <b>AK Kar, GS More, R Srivastava</b> - Catalysis in Confined Frameworks: Synthesis, Characterization, and Applications: Book Chapter, 2023</p> <p><b>Abstract</b>  The endless structural features make the metal-organic framework (MOF) one of the promising classes of modern-day material. The basic features associated with MOF structure are high surface area, unique structural properties, and tunable chemical functionality. MOF is a highly crystalline material with a large surface area and a diverse range of tailorable porous framework structures. The porous framework structure of MOF arises due to the self-assembly of organic linkers (ligands) and metal nodes. Therefore, the possible active sites in MOF are located near the pores, metal nodes, and ligand centers. The functional tunable properties of MOF provide numerous opportunities for structural modifications and make them ideal for highly efficient catalytically active material by active site engineering of pores, metal nodes, and ligand centers. The resultant structurally modified MOFs are a unique class of catalytic material and have been successfully employed in several heterogeneous catalytic transformations. Additionally, MOF tends to carry homogeneously distributed metallic sites or other nanoscopic guest particle as the additional active centers, which can be used for a selected appointed catalytic reaction. The major challenges associated with the structurally modified MOF through active site engineering are their controlled synthesis strategies, the exact estimation of the modifications, and the apparent stability of the modified MOF. The idea of MOF framework modification is attributed to the modifications in the physical and chemical environment of the framework regions where the framework stability and reactivity altered and ultimately brought different interactions with the target species for organic transformation.</p>
25.	<p><a href="#">EQBAL-RS: Mitigating popularity bias in recommender systems</a>  <b>S Gupta, K Kaur, S Jain</b> - Journal of Intelligent Information Systems, 2023</p> <p><b>Abstract:</b>  Recommender systems are deployed heavily by many online platforms for better user engagement and providing recommendations. Despite being so popular, several works have shown the existence of popularity bias due to the non-random nature of missing data. Popularity bias leads to the recommendation of only a few popular items causing starvation of many non-popular items. This paper considers an easy-to-understand metric to evaluate the popularity bias as the difference between mean squared error on popular and non-popular items. Then, we propose EQBAL-RS, a novel re-weighting technique that updates the weights of popular and non-popular items. Re-weighting ensures that both item sets are equally balanced during training using a trade-off function between overall loss and popularity bias. Our experiments on real-world datasets show that EQBAL-RS outperforms the existing state-of-art algorithms in terms of accuracy, quality, and fairness. EQBAL-RS works well on the proposed and existing popularity bias metrics and has significantly reduced runtime. The code is publicly available at <a href="https://github.com/eqbalrs/EqBalRS">https://github.com/eqbalrs/EqBalRS</a></p>
26.	<p><a href="#">Flexible electrochemical sensor for highly sensitive and selective non-enzymatic detection of creatinine via electrodeposited copper over polymelamine formaldehyde</a>  <b>D Mehta, A Kifle, TC Nagaiah</b> - Journal of Materials Chemistry B, 2023</p> <p><b>Abstract</b>  A non-enzymatic electrochemical biosensor was developed for highly sensitive detection of creatinine using copper nanoparticles supported over polymelamine formaldehyde. The</p>

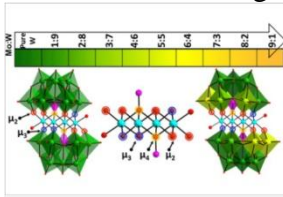
	<p>synergy between the electrodeposited copper nanoparticles over the highly porous polymer (eCu-PMF) provided a greener platform to boost up the electron transport at the electrode electrolyte interface by eliminating the role of redox species as well as interference of major interferents like glucose, dopamine, and ascorbic acid in physiological media 0.1 M PBS (pH 7.4). The proposed sensor exhibited a wide detection range of 100 fM-60 mM with high sensitivities of 0.320 mA nM<sup>-1</sup> cm<sup>-2</sup> and 3.8 mA nM<sup>-1</sup> cm<sup>-2</sup>. Moreover, the sensor was applied to real samples of serum creatinine and recoveries of 97 to 114% were found. Additionally, a paper-based flexible screen-printed electrode was fabricated which displayed an excellent activity with the same detection range of 100 fM-60 mM and long-term storage stability of 15 days.</p>
27.	<p><a href="#">Functionalized imidazolium/benzimidazolium-derived ionic liquid-based materials for biomedical applications</a>  <b>D Bains, G Singh, N Kaur, N Singh</b> - Advanced Materials for Biomedical Applications: Book Chapter, 2023</p> <p><b>Abstract</b>          Ionic liquids (ILs) are composed of organic cations, associated with an organic or inorganic anion exhibiting unique physiochemical properties including low toxicity, low vapor pressure, good chemical stability, good thermal stability, and tunable solubility, and considered as a green solvent in recent years.</p>
28.	<p><a href="#">Homotopy analysis method and its convergence analysis for a nonlinear simultaneous aggregation-fragmentation model</a>  <b>S Yadav, S Keshav...</b> <b>J Kumar</b> - Chaos, Solitons &amp; Fractals, 2023</p> <p><b>Abstract</b>          In this article, we focus on addressing the missing convergence analysis of the homotopy analysis method (HAM) for solving pure aggregation and pure fragmentation population balance equations [Kaur et al. (2023), J. Math. Anal. Appl., 512(2), 126166]. This technique is further extended to determine analytical series solutions for a simultaneous aggregation–fragmentation (SAF) population balance equation. The convergence analysis of the extended approach for a SAF equation is performed using the concept of contraction mapping in the Banach space. The HAM method enables us to derive recursive formulas to obtain series solutions, distinguishing it from traditional numerical approaches. One noteworthy advantage of HAM is its capability to solve both linear and nonlinear differential equations without resorting to discretization, while incorporating a convergence control parameter. Given the complex nature of the SAF equation, only a single analytical solution has been available, specifically for a constant aggregation kernel and a binary breakage kernel with a linear selection function. However, our study presents new series solutions for the number density functions, considering the combination of sum and product aggregation kernels with binary breakage kernels and linear/quadratic selection functions. These particular solutions have not been previously documented in the existing literature. To verify the accuracy and efficiency of the proposed approach, the results with the finite volume scheme [Singh et al. (2021), J. Comput. Phys., 435, 110215] for establishing the accuracy and effectiveness of the proposed approach.</p>
29.	<p><a href="#">Influence of van der waals interactions between the alkyl chains of surface ligands on the size and size distribution of nanocrystals prepared by the digestive ripening process</a>  <b>JR Shimpi, R Thomas, SK Meena</b> - Langmuir, 2023</p> <p><b>Abstract</b>          Thermal heating of polydispersed nanocrystals (NCs) with surface-active organic ligands in a solvent leads to the formation of monodispersed NCs, and this process is known as digestive ripening (DR). Here, by performing DR on Au NCs using different-chain-length amine and thiol</p>

	<p>ligands, we evidently show that ligands with C12 chain length result in the formation of NCs with narrow size distributions when compared to C8, C16, and C20 chain length ligands. Furthermore, our findings also show that in the case of alkyl thiol, the NC size remains more or less the same, while the size distribution gets altered significantly with the chain length. On the other hand, both size and size distribution are affected significantly when the alkyl amine chain length is varied. Fourier transform infrared (FTIR) studies indicate that the van der Waals (vdW) interactions are weakest when the amine with C12 carbon chain is used as the DR agent, while in the case of thiols, molecules with C8 and C12 chain lengths have nearly the same vdW interactions (with C12 slightly weaker than C8), which are weaker than those of C16 and C20. Molecular dynamics (MD) simulation results corroborate the experimental observations and suggest that due to more defects in the alkyl chain, the C8 and C12 (amine as well as thiol) ligands are disordered and less stable on Au(111) and Au(100) surfaces. This could result in efficient etching and redeposition, making the ligands with C8 and C12 chain lengths the better DR agents.</p>
30.	<p><a href="#">Interfacial molecular structure of phosphazene-based polymer electrolyte at the air-aqueous interface using sum frequency generation vibrational spectroscopy</a>  <b>S Kaur, D Tomar, M Chaudhary, B Rana, H Kaur.... KC Jena - Journal of Physics: Condensed Matter, 2023</b></p> <p><b>Abstract</b>  The change induced in the physicochemical properties of polymer while hosting ions provides a platform for studying its potential applications in electrochemical devices, water treatment plants, and materials engineering science. The ability to host ions is limited in very few polymers, which lack a detailed molecular-level understanding for showcasing the polymer-ion linkage behavior at the interfacial region. In the present manuscript, we have employed sum frequency generation (SFG) vibrational spectroscopy to investigate the interfacial structure of a new class phosphazene-based methoxyethoxyethoxyphosphazene (MEEP) polymer in the presence of lithium chloride salt at the air-aqueous interface. The interfacial aspects of the molecular system collected through SFG spectral signatures reveal enhanced water ordering and relative hydrogen bonding strength at the air-aqueous interface. The careful observation of the study finds a synchronous contribution of van der Waals and electrostatic forces in facilitating changes in the interfacial water structure that are susceptible to MEEP concentration in the presence of ions. The observation indicates that dilute MEEP concentrations support the role of electrostatic interaction, leading to an ordered water structure in proximity to diffused ions at the interfacial region. Conversely, higher MEEP concentrations promote the dominance of van der Waals interactions at the air-aqueous interface. Our study highlights the establishment of polymer electrolyte characteristics mediated by intermolecular interactions, as observed through the spectral signatures witnessed at the air-aqueous interface. The investigation illustrates the polymer-ion linkage adsorption effects at the interfacial region, which explains the macroscopic changes observed from the cyclic voltammetry studies. The fundamental findings from our studies can be helpful in the design and fine-tuning of better polymer electrolyte systems that can offer improved hydrophobic membranes and interface stability for use in electrochemical-based power sources.</p>
31.	<p><a href="#">Introducing N-sulfinylamines into visible-light-induced carbene chemistry for the synthesis of diverse amides and <math>\alpha</math>-iminoesters</a>  <b>S Roy, A Biswa, H Paul, S K Ariyan, I Chatterjee - Organic Letters, 2023</b></p> <p><b>Abstract</b>  A rare example of visible-light-mediated diverse reactivity of N-sulfinylamines with different types of carbene precursors has been disclosed. Acylsilanes and aryldiazoacetates have been utilized as nucleophilic and electrophilic carbene precursors into the N=S=O linchpin, to achieve valuable amides and <math>\alpha</math>-iminoesters, respectively. Interestingly, diazocarbonyls can also</p>

	<p>participate in the amidation reaction with N-sulfinylamines via in situ generated ketenes. This operationally simple modular method offers a mild, transition-metal-free, and coupling-reagent-free protocol to fabricate structurally diverse amides and a promptly accessible technique to achieve <math>\alpha</math>-iminoesters, where visible light remains as a key promoter.</p>
32.	<p><a href="#">Mapping complete eigensolution space for the analysis of stress transfer in and around the broken fiber: A variational principle based approach</a>  <b>AV Sirsat, SS Padhee</b> – Journal of Composite Materials, 2023</p> <p><b>Abstract</b>  One of the critical reasons for the failure of the Fiber Reinforced Composite (FRC) is fiber breakage. The stress transfer in and around this breakage has remained the topic of research for the last couple of decades. The two-phase composite model is generally considered standard to gain insight into the mechanics. Most of the literature simplifies the problem by considering the shear lag approximations or some other a-prior and/or ad hoc assumptions on various field variables. Moreover, the majority of the study in the literature considers both matrix and fiber to be isotropic. On the contrary, most of the fibers in FRC are transversely isotropic. In the present manuscript, an attempt has been made to provide a solution for this problem with an anisotropic fiber satisfying all the boundary conditions and continuity requirements in an exact sense. The solution strategy adopts the derivation of the solution for individual phases under axial traction and then imposes the boundary and the continuity conditions. The formulation of the problem for the individual phase is based on the variational principle and the solution is based on the method of separation of the variables and the Frobenius method. To validate the solution the numerical results for the various stresses have been compared against the results from the Finite Element Analysis (FEA). The comparison shows a good agreement between them. Further, the effect of the volume fraction and the fiber-matrix stiffness ratio on the Ineffective length, maximum shear stress at the interface, and the far-field stresses in the fiber has been studied.</p> <p><b>Author keywords</b>  Anisotropic materials; axisymm</p>
33.	<p><a href="#">MFC: A multishot approach to federated data clustering</a>  <b>J Makkar, Bhumika, S Jain, S Gupta</b> - Frontiers in Artificial Intelligence and Applications: Conference Paper, 2023</p> <p><b>Abstract</b>  The work explores the federated data clustering problem. The primary goal is to perform k-means clustering of data distributed over multiple clients while preserving privacy during an exchange with the central server. Existing solutions to unsupervised federated data clustering are either computationally challenging or effective only in heterogeneous regimes, i.e., when the number of clusters per client (<math>k_z</math>) is less than the total number of clusters (<math>k</math>) (specifically, <math>k_z \leq k</math>). Moreover, existing one-shot approaches assume that the information about <math>k_z</math> is available for each client. In this paper, we propose two multi-shot approaches which we call MFC and MFCH, that perform well on both heterogeneous and non-heterogeneous regimes, i.e., are independent of the underlying client data distribution. Both MFC and MFCH stand out as they do not rely on prior knowledge about <math>k_z</math>. We theoretically bound the closeness of the local centers obtained by MFC to that of the optimal global centers and prove that under some well-separability assumption, the centers will be close enough. MFCH improvises MFC by only sharing a single cluster center from each client, thus ensuring more privacy. Our theoretical analysis shows that when at least <math>O(k^2 \log k)</math> clients are involved, centers obtained by MFCH will closely approximate optimal global centers. Experiments on synthetic and real-world datasets validate the proposed approaches' efficacy showcasing lower objective costs in non-heterogeneous regimes while</p>



	<p>having comparable performance in heterogeneous regimes. In addition, as a byproduct MFC exhibits higher device-level fairness in terms of the individual objective cost compared to existing state-of-the-art algorithms. The code is publicly available at <a href="https://github.com/shivi98g/MFC">https://github.com/shivi98g/MFC</a>.</p>
34.	<p><a href="#">Microstructural and Mechanical Properties of Cr-Ni3Al Alloy Films Synthesized by Magnetron Sputtering</a>  SK Tiwari, AU Rao, AS Kharb...N Sardana - Journal of Materials Engineering and Performance, 2023.</p> <p><b>Abstract</b>  Cr-Ni3Al alloy films have been deposited on Si (100) substrate via DC magnetron sputtering. The effect of Cr enrichment on microstructure and mechanical properties has been studied. The evolution of phases, microstructure, surface topography and mechanical properties has been studied using GI-XRD, FE-SEM, AFM and quasi-static nanoindentation, respectively. Results revealed that the alloy films possessed a preferred orientation of (111) plane with a maximum hardness and Young's modulus of ~12.7 GPa and ~203 GPa for 0 W Cr-Ni3Al films which further decreased to ~7 GPa and 129 GPa, respectively, for 40 W Cr-Ni3Al films. The reported values of hardness and Young's modulus are very high in the case of alloy Ni3Al-based coatings when compared with the literature. This study also imitates that with the increase in Cr concentration in the host Ni3Al matrix, the surface roughness increased as a result of the evolution of pores. However, hydrophobicity is observed to be increased with increase in Cr concentration in host Ni3Al coatings with a maximum contact angle of 115.9° for 40 W Cr-Ni3Al alloy film.</p> 
35.	<p><a href="#">Minimizing environmental degradation in fracture toughness of carbon fiber/epoxy composites using carbon nanotubes</a>  A Yesu, M Srivastava, PK Agnihotri... – Engineering Fracture Mechanics, 2023</p> <p><b>Abstract</b>  Environment assisted degradation in mechanical properties is a major concern for the integrity of composites in structural applications. Experiments are performed to examine the efficacy of carbon nanotubes (CNTs) to counter the adverse effect of environmental conditions on the fracture toughness of carbon fiber/epoxy composites (CFRP). Composite coupons are exposed to accelerated weathering cycle for varying durations. Experimental testing shows that the fracture toughness degrades significantly after exposure to aging cycle. The addition of CNTs minimizes the adverse effect of weathering. The comparable fracture toughness of 1000 hrs aged CNT modified CFRPs with the unaged conventional CFRPs suggest that the advantages of CNT addition persist even after exposure to prolong weathering conditions. Fractography analysis reveals that the CNT induced toughening of epoxy improves Mode I and Mode II fracture toughness of conventional CFRPs. While the fracture in conventional CFRP is primarily at fiber/matrix interface, textured microflow, larger sized cusp and matrix cracking are observed in CNT modified CFRPs.</p>
36.	<p><a href="#">Mitigation of wave force on a tunnel in the presence of submerged porous plate over trench-type bottom topography</a>  S Choudhary, SC Martha - Journal of Offshore Mechanics and Arctic Engineering, 2023</p> <p><b>Abstract</b>  Thin porous plates serve as an effective model for the construction of breakwater. Thus, the</p>

	<p>problem involving oblique wave interaction with a tunnel in the presence of a submerged horizontal porous plate over a trench-type bottom is investigated. In this paper, for the mathematical formulation of the physical model, water wave potentials are defined using Havelock's expansions and flow past over porous structure is modelled based on Darcy's law. The advantage of the trench type of bottom and horizontal plate are studied through the numerical results of forces on the tunnel. The study reveals that more energy loss and less force on the tunnel are obtained if the porous effect parameter of the plate or the length of the plate is increased up to a moderated value of these parameters. Compared to the case without porous plate and trench-type bottom topography, there are significant changes in forces due to this porous breakwater and trench-type bottom topography. In addition, from the present results, it may be noted that the load on the submerged tunnel is reduced by adding a submerged horizontal porous plate and asymmetric trench, which is helpful in understanding the role of porous breakwaters and trenches in applications to Ocean and Coastal Engineering.</p>
37.	<p><a href="#">Modulation of the Band Gap and Redox Properties by Mixed Addenda in Sandwich Polyoxometalates</a>  <b>G Singh, D Mandal</b> - Inorganic Chemistry, 2023</p> <p><b>Abstract</b>  Due to the wide range of applications of band-gap engineering in optoelectronics and photocatalysis, the rational design of polyoxometalate (POM) frameworks is highly desired. Here, we have successfully synthesized a series of mixed addenda (Mo and W) sandwich POMs by systematically varying pH, concentrations of salts, and counterions in Weakley-type sandwich POMs by incorporating Mo into the framework of tetrasubstituted sandwich POMs. Crystallographic analysis reveals the centrosymmetric structure; with variation in the Mo to W ratio, Mo preferentially binds to <math>\mu_2</math> oxygen connected to transition metals in the sandwich position. UV–visible spectroscopy, electrochemical, and theoretical modeling rationalize the band-gap modulations. Theoretical studies and cyclic voltammograms indicate that during the reduction, the incoming electrons preferentially go to substituted transition metals followed by Mo. Flat band potential calculated from the Mott–Schottky enables tuning of the electronic properties of composites based on these sandwich POMs. Moreover, the dioxygen binding and activation studies of these polyoxometalates have been highlighted.</p> 
38.	<p><a href="#">Multi-dimensional population balance modeling of sonocrystallization of pyrazinamide with systematic estimation of kinetic parameters based on uncertainty and sensitivity analyses</a>  <b>A Maharana, P Sehrawat, A Das, J Kumar, D Sarkar</b> - Chemical Engineering Research and Design, 2023</p> <p><b>Abstract</b>  Application of ultrasound has several beneficial effects on both crystallization process and product crystal properties. This work focuses on experimental study and population balance modeling of ultrasound-assisted unseeded batch cooling crystallization of an important polymorphic pharmaceutical. The <math>\delta</math>-polymorph of pyrazinamide, a drug for mycobacterium tuberculosis, exhibits plate-like morphology, and such crystals are best described by at least two dimensions: length and width. A multi-dimensional population balance model for batch cooling sonocrystallization of pyrazinamide from its 1,4-dioxane solution is developed and validated. A series of experiments are performed with different ultrasound amplitudes (silent, 10%, and 50%) to study the effect of ultrasound on nucleation rate, crystal size, and polymorphism. The ultrasound is applied till the point of nucleation and an enhanced nucleation rate is introduced in</p>

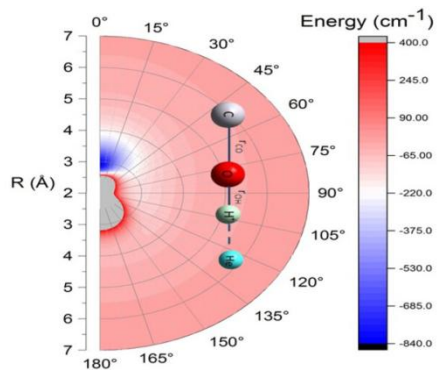
	<p>the model in the presence of ultrasound irradiation. The various kinetic parameters are estimated following a systematic methodology based on uncertainty quantification and sensitivity analysis using experimental observations related to solute concentration and crystal size distribution. The Polynomial Chaos Expansion (PCE) is used to quantify the uncertainties in model prediction due to kinetic parameter uncertainties and sensitivity analysis is performed using total order Sobol's sensitivity indices derived from PCE model. The kinetic parameters are estimated in two steps. First, a global search technique is used to simultaneously estimate all the kinetic parameters. Next, the less sensitive parameters are kept fixed and the more significant parameters are fine-tuned using a gradient-based local optimizer. Out of total nine kinetic parameters, only four parameters appeared to be significant for both silent and sonicated cases. The high-resolution finite volume scheme is used to solve the multi-dimensional population balance model and the simulation results agree very well with experimental data related to both concentration and crystal size distributions. The results revealed that compared to silent cases, sonication increased the nucleation rate by <math>10^2</math> times and <math>10^4</math> times for 10% and 50% amplitude, respectively. The growth rate was also enhanced significantly with increase in ultrasonic amplitude. All the experiments yielded the desired <math>\delta</math>-polymorph of pyrazinamide.</p>
39.	<p><a href="#">On the role of vacancy-hydrogen complexes on dislocation nucleation and propagation in metals</a>  <b>A Arora, H Singh, I Adlakha, DK Mahajan</b> - <i>Modelling and Simulation in Materials Science and Engineering</i>, 2023</p> <p><b>Abstract</b>  New insights are provided into the role of vacancy-hydrogen (VaH) complexes, compared to the hydrogen atoms alone, on hydrogen embrittlement of nickel. The effect of the concentration of hydrogen atoms and VaH complexes is investigated in different crystal orientations on dislocation emission and propagation in single crystal of nickel using atomistic simulations. At first, embrittlement is studied on the basis of unstable and stable stacking fault energies as well as fracture energy to quantify the embrittlement ratio (unstable stacking fault energy/fracture energy). It is found that VaH complexes lead to high embrittlement compared to H atoms alone. Next, dislocation emission and propagation at pre-cracked single crystal crack-tip are investigated under Mode-I loading. Depending upon the elastic interaction energy and misfit volume, high local concentrations at the crack front lead to the formation of nickel-hydride and nickel-hydride with vacancies phases. These phases are shown to cause softening due to earlier and increased dislocation emission from the interface region. On the other hand, dislocation propagation under the random distribution of hydrogen atoms and VaH complexes at the crack front or along the slip plane shows that VaH complexes lead to hardening that corroborates well with the increased shear stresses observed along the slip plane. Further, VaH complexes lead to the disintegration of partial dislocation and a decrease in dislocation travel distance with respect to time. The softening during emission and hardening during propagation and disintegration of partial dislocation loops due to VaH complexes fit the experimental observations of various dislocation structures on fractured surfaces in the presence of hydrogen, as reported in literature.</p>
40.	<p><a href="#">One pot synthesis of hydrogen and glucaric acid via glucose electrolysis</a>  <b>D Mehta, S Kaur, N Thakur, TC Nagaiah</b> - <i>Journal of Materials Chemistry A</i>, 2023</p> <p><b>Abstract</b>  Amidst the rising population and energy demands, hydrogen fuel provides a cleaner, greener, and more sustainable alternative to fossil fuels. In this aspect, electrochemical oxidation of biomass such as glucose, affords a more energy-efficient method as compared to water electrolysis in terms of energy storage, enhanced hydrogen (<math>H_2</math>) production and production of a value-added fuel viz. glucaric acid. Herein, we have designed nickel manganese oxide over OCNT as a bifunctional electrocatalyst for hydrogen evolution reaction (HER) at the cathode and glucose oxidation reaction (GOR) at the anode. While assembled a full cell (GOR-HER), 370 mV of potential was saved and a boost in hydrogen production from <math>0.05 \text{ mL min}^{-1}</math> to <math>0.16 \text{ mL min}^{-1}</math>.</p>

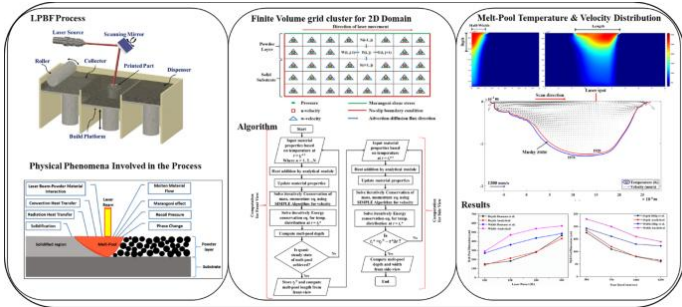
	<p><math>\text{min}^{-1}</math> was recorded. Moreover, selective formation of glucaric acid was confirmed by HR-MS, <math>^1\text{H}</math>-NMR and <math>^{13}\text{C}</math>-NMR with a F.E. of 62.8% at 1.3 V vs. RHE.</p>
41.	<p><a href="#">Operando scanning electrochemical microscopic investigation and visualization of NRR-HER competition in electrochemical <math>\text{NH}_3</math> synthesis</a>  <b>D Gupta, A Kafle, M Singh, D Dahare TC Nagaiah</b> – Journal of Materials Chemistry A, 2023</p> <p><b>Abstract</b>          Electrochemical dinitrogen reduction (NRR) has emerged as one of the most promising potential alternatives to the energy-intensive Haber-Bosch process for clean and carbon-free ammonia (<math>\text{NH}_3</math>) production. However, the major setback in this electrochemical synthesis is the selectivity between NRR and the competing hydrogen evolution reaction (HER) that leads to poor faradaic efficiency. The competition between NRR and HER is underexplored, and the existing ex situ <math>\text{NH}_3</math> and <math>\text{H}_2</math> detection methods do not provide the real-time detection of products formed near the electrode surface with high spatial resolution. Therefore, the operando investigation of <math>\text{NH}_4^+</math> production during electrochemical <math>\text{N}_2</math> reduction and its competition with HER was demonstrated using scanning electrochemical microscopy (SECM) via the sample generation-tip collection (SG-TC) mode. A distinct net current density difference was observed at an Au-ultramicroelectrode (UME) during sequential chronoamperometry and the visualization of local catalytic activity over the catalyst in Ar- and <math>\text{N}_2</math>-saturated electrolytes. Therefore, this study provides invaluable information on the competition between the NRR and the HER at applied potentials within milliseconds and also visualization with high spatial resolution and accuracy.</p>
42.	<p><a href="#">Optimization of bio-ink using machine learning</a>  <b>A Mukherjee, S Sarker, R Kumar, A Sahani, B Das</b> -Artificial Intelligence in Tissue and Organ Regeneration: Book Chapter, 2023</p> <p><b>Abstract</b>          Bioprinting is one of the most advanced manufacturing techniques for the fabrication of biological tissue equivalents. The technique has immense potential in the area of biofabrication, especially in the area of tissue engineering, artificial organs, and in vitro 3D model development for drug screening. However, a major lacuna of bioprinting is the requirement of specialized biomaterial cell composite development which has printability. The components of bio-ink include biopolymers, cells, growth factors, etc. Most of these components are costly, and it takes multiple experiments to optimize the composition and reproducibility. Thus, a machine learning model can be highly useful for the optimization of the bio-ink. The current chapter focuses on the different characteristics or parameters important for bio-ink formulation and different machine-learning tools to optimize bio-ink composition.</p>
43.	<p><a href="#">Parameters affecting the efficiency of extraction systems in the food industries</a>  <b>S Bhokariker, P Poojitha, V Vaishampayan, A Sridhar...</b> - Extraction Processes in the Food Industry: Book Chapter, 2024</p> <p><b>Abstract</b>          Extraction is a critical step in phytochemical and food processing for the bioactive elements from plant materials. Additives extracted from plants could be used in nutraceuticals and functional foods. Functional foods, minimally processed food, and nutraceuticals are no longer choices for health-conscious people but a need for everyone. Consumers these days are highly reliant on ready-to-eat and processed food products hence modern technologies should be able to extend shelf life. The use of sustainable and environment-friendly technologies in the food and pharmaceutical industries has been constantly growing worldwide in comparison to conventional technologies. Development of advanced technologies which guarantee the long-term survival of the human species and fulfill the requirements of food demands due to increased population is essential. Emerging new technologies are able to replace traditional thermal and chemical treatments for extraction without any nutrient loss or unpleasant change in the sensory properties of a food product. The selection of appropriate extraction methods and standardization of parameters for the optimization of the process is crucial for up-scaling in the industries. Industry-oriented research with a</p>

	<p>global approach is required to speed up the implementation of technology to meet the demands of the food industry as well as to troubleshoot the problems caused during processing. This chapter aims to provide a summary of conventional and non-conventional extraction methodologies. Further, various factors such as solvent selection, temperature, pressure, electric field, specific energy, enzymes, and so on that affect the efficiency of various non-conventional extraction techniques have been discussed thoroughly.</p>
44.	<p><a href="#">Particle shape matters: Flow and heat transfer characteristics of nonspherical particles</a>  <b>P Suri, SA Patel</b> - Powder Technology, 2023</p> <p><b>Abstract</b>  The primary shape considered for the present numerical study is the spherical segment dissected from the spherical particle at an angle <math>\alpha</math> from its vertical y-axis. The shape effect of the spherical segments on momentum and heat transfer characteristics are presented in terms of shape factor (<math>\psi</math>) spanning over the range of <math>0.424 (\alpha = 30^\circ) \leq \psi \leq 0.996 (\alpha = 150^\circ)</math> for Reynolds number, <math>1 \leq Re \leq 150</math>. The results of drag, heat transfer coefficient, and streamlines have been compared with the closest shapes of spherical segment, i.e., cone (<math>0.324 \leq \psi \leq 0.658</math>) and short cylinder (<math>0.541 \leq \psi \leq 0.872</math>) to identify the role of the particle shape. The range of shapes has been correlated for drag and average Nusselt number as a function of Re, shape factor, <math>\psi</math> and particle longest chord length or base diameter to height ratio (<math>1 \leq d_c/h \leq 7.463</math>).</p>
45.	<p><a href="#">Phonon-mediated superconductivity in <math>Mg_{1-x}Mo_xB_2</math> compounds: a crystal prediction via cluster expansion and particle-swarm optimization</a>  <b>P Tsuppayakorn-aek, W Luo, R Ahuja...</b> - Scientific Reports, 2023</p> <p><b>Abstract</b>  Investigating superconductivity represents one of the most significant phenomena in the field of condensed matter physics. Our simulations aim to elucidate the structures in the metallic state of <math>Mg_{1-x}Mo_xB_2</math>, which is essential for predicting their superconducting properties. By employing a first-principle cluster expansion and particle-swarm optimization, we have predicted the structures of <math>Mg_{1-x}Mo_xB_2</math> ternary alloys, including <math>Mg_{0.667}Mo_{0.333}B_2</math>, <math>Mg_{0.5}Mo_{0.5}B_2</math>, and <math>Mg_{0.333}Mo_{0.667}B_2</math>, and have determined their thermodynamically stable configurations under both atmospheric and high-pressure conditions. To investigate the potential for superconductivity in these structures, we have conducted a detailed examination of electronic properties that are pertinent to determining the superconducting state. Regarding superconducting properties, <math>Mg_{0.333}Mo_{0.667}B_2</math> exhibits superconductivity with a critical temperature (<math>T_c</math>) of 7.4 K at ambient pressure. These findings suggest that the theoretically predicted structures in Mg/Mo-substituted metal borides could play a significant role in synthesis and offer valuable insights into superconducting materials.</p>
46.	<p><a href="#">Polymer-derived SiOC ceramic coating for corrosion protection</a>  <b>R Bura, B Kumar, RM Prasad</b> - International Journal of Applied Ceramic Technology, 2023</p> <p><b>Abstract:</b>  In the present study, a polymer-derived silicon oxycarbide (SiOC) ceramic layer has been coated on stainless steel 304 (SS304) to improve corrosion resistance in a seawater environment. The surface of SS304 is dip-coated with vinyl-functionalized polysiloxane, followed by pyrolysis under argon at 800°C to obtain SiOC layer with a thickness of about 1 <math>\mu</math>m after two-fold coating/pyrolysis steps. Structural characterization of the samples was performed by fourier transform infrared (FTIR), X-ray diffraction, Raman spectroscopy, and scanning electron microscopy. Electrochemical characterization of SS304 and SiOC-coated SS304 is performed in 0.6 M NaCl solution. Potentiodynamic polarization measurements showed improved corrosion resistance of SiOC-coated SS304 with a very low corrosion current density of <math>4.14 \times 10^{-9}</math> A/cm<sup>2</sup> whereas for uncoated SS304 corrosion current density of <math>4.56 \times 10^{-7}</math> A/cm<sup>2</sup> was measured. Electrochemical impedance spectroscopic study confirmed superior corrosion resistance behavior of SiOC-coated SS304 over uncoated SS304.</p>
47.	<p><a href="#">Probabilistic algebraic attack on plantlet lightweight stream cipher</a>  <b>DK Sharma, R Pandey, T Chatterjee</b> - Sadhana - Academy Proceedings in Engineering Sciences, 2023</p>



	<p><b>Abstract</b></p> <p>Plantlet is a new variant of Sprout lightweight stream cipher. It uses 61 bit LFSR and 40 bit NFSR. This paper presents a study of Plantlet stream cipher with probability based approach for making algebraic attack on Plantlet. In this paper, we have used low degree multiple of Boolean function to apply algebraic attack. The low degree multiple of Boolean function is multiplied to output keystream function in order to get output equation such that it consists of only LFSR state variables. These equations are further solved to find secret key and internal states. In this manner, the complexity of solving equations is reduced. In this paper, it takes <math>2^{60.99}</math> Plantlet encryptions to solve system of equations. Commonly, standard algebraic attack and fast algebraic attack have been applied on various stream ciphers. However, the probabilistic algebraic attack has been implemented on Grain family of stream ciphers but not on Plantlet. The probabilistic algebraic attack can be applied on other stream ciphers. © 2023, Indian Academy of Sciences.</p> <p><b>Author keywords</b></p> <p>algebraic attack; Boolean function; lightweight stream cipher; linear feedback shift register; low degree multiple; nonlinear feedback shift register</p>
48.	<p><a href="#">Radish plant growth monitoring using multimodal fusion</a>  <b>S Bansal, M Singh, S Barda, V Kumar, N Goel, M Saini</b> - IEEE Conference on AgriFood Electronics (CAFE), 2023</p> <p><b>Abstract</b></p> <p>In the realm of precision agriculture, successful plant growth monitoring plays a pivotal role, and it is greatly aided by advanced deep learning techniques utilizing data from various sensors. The key objective of the paper is to develop a model to monitor the growth of the radish plant through the integration of multi-modal data, specifically RGB and Depth (RGB-D) images. Plant growth can be modeled based on many parameters, for example, the height of the plant, the environmental conditions (such as temperature, humidity, and light intensity), nutrient levels in the soil, leaf count, and the presence of pests or diseases, etc. The proposed study estimates the age of the radish plant with an end-to-end deep-learning model. We developed a Fused Image Transformer (FIT) model to estimate the age of the plant in weeks. The FIT uses a self-attention mechanism to estimate the essential features of the images which will help to complete the objective. The proposed method is compared with the state-of-the-art models for regression problems. We have also validated the FIT model with or without depth information. The Mean squared loss with and without depth information is found to be 0.025 weeks and 2.059 weeks respectively which shows a significant improvement by using the depth information.</p>
49.	<p><a href="#">Rice Husk: From Agro-Industrial to Modern Applications</a>  <b>S Mishra, I Dhada, P Haldar</b> - Agricultural Waster to Value-Added Products, 2023</p> <p><b>Abstract</b></p> <p>The concept of a circular bioeconomy is getting developed due to exhaustiveness of natural resources and exorbitant waste production. The use of valuable by-products assures to shore up and escalate environmental sustainability. Worldwide production of rice accounts for more than 750 million grain tons and 150 million husk tons annually. Rice husk contains valuable biomaterials, each of which has extensive applications in various fields (23–35% cellulose, 26–31% lignin, 18–21% hemicellulose, 15% pentosans, 16% minerals including silica). Although rice husk is a rich source of valuable and widely used materials, unfortunately it is still not widely used in the world. In this chapter, its industrial applications are mentioned to promote its use on a large scale. The proportions of each component depend primarily on rice genotype, soil chemistry, and climatic conditions. Rice husk (RH) and its derivatives, such as rice husk ash (RHA), rice husk biochar (RHB), rice husk hydrochar (RHH), and activated carbon (RHAC), have been placed forefront for applications in agriculture and other industries. While the</p>

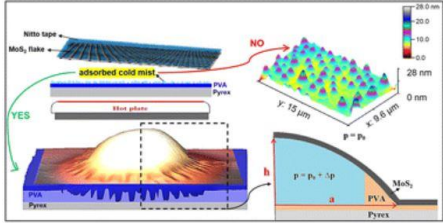
	<p>investigation of RH's composition, microstructure, and by-products has been done intensively, owing to its unique characteristics, it is still an open-ended area with numerous scopes for research, particularly in identifying RH potential applications. Hence, disregarding the environmental effects, the production of value-added products and RH applications in various industries are in the spotlight. A comprehensive review of RHA, RHB, RHH, and RHAC obtainment and their applications in various fields (including fuel and other energy resources, construction materials (concrete and firebrick), pharmacy, medicinal uses, and nanobiotechnology) is the focus of this chapter.</p>
50.	<p><a href="#">Rotational transitions of COH<sup>+</sup> and He: new interaction potential, bound states, scattering and pressure broadening cross-sections</a>  <b>Ritika, TJ Dhilip Kumar</b> – ChemPhysChem, 2023</p> <p><b>Abstract</b>  We present new calculations of a metastable isomer of HCO<sup>+</sup>, i. e., COH<sup>+</sup> in collision with He. The COH<sup>+</sup> has been suggested as an alternative molecular hydrogen tracer, which makes it of great interest for astrophysical studies. COH<sup>+</sup> was first observed in astronomical space towards SgrB2 with the observation of <math>J=1\rightarrow0</math>, <math>J=2\rightarrow1</math> and <math>J=3\rightarrow2</math> lines. Calculations are based on new <i>ab initio</i> potential energy surfaces (PES) of charged complex COH<sup>+</sup>-He using the CCSD(T) in conjunction with aug-cc-pVQZ basis set. The PES has a well depth of <math>-836.5\text{ cm}^{-1}</math> towards H-end at the COH<sup>+</sup>-He distance (<math>R</math>) of <math>2.9\text{ \AA}</math> in linear orientation. To test the new PES, the calculations of the bound-state are carried out and pressure broadening cross-sections of COH<sup>+</sup> with He collisions are computed for kinetic energies up to <math>150\text{ cm}^{-1}</math> using the accurate close-coupling method. Further, the pressure broadening and shift coefficients have been calculated from the corresponding real and imaginary parts of cross-sections for the first six rotational transitions. The data obtained is found to be in the same order as the HCO<sup>+</sup>-He system. Further, the results of rate coefficients are compared with the reported COH<sup>+</sup>-He and HCO<sup>+</sup>-He data. The results generated by this study are believed to be useful for both laboratory and future astrophysical research.</p> <p><b>Graphical Abstract</b>  To determine an accurate abundance of COH<sup>+</sup> in the interstellar medium, its electronic structure calculations are performed with helium in this study. Bound states and pressure broadening calculations are done for the COH<sup>+</sup>-He complex.</p> 
51.	<p><a href="#">Semi-analytical formulation for single-track laser powder-bed fusion process to estimate melt-pool characteristics considering fluid-flow and marangoni effect</a>  <b>D Bombe, R Kumar, SK Nandi, A Agrawal</b> - International Journal on Interactive Design ..., 2023</p> <p><b>Abstract</b>  The Laser-Based Powder Bed Fusion (LPBF) process is an additive manufacturing (AM) technique used to fabricate intricate 3D metallic components from fine powder particles. This study presents a 2D semi-analytical model, an algorithm developed by incorporating multiple physical phenomena of the process, i.e., heat transfer, fluid flow, and Marangoni effect for computing temperature and velocity distribution, to estimate the melt-pool characteristics for the single-track melting. The laser input energy has been modelled as a moving Gaussian volumetric heat source, and the fluid flow phenomenon has been formulated by 'Semi-Implicit Method for</p>

	<p>Pressure Linked Equations' (SIMPLE) method. A set of two-dimensional transient conservation of mass, momentum, and energy equations are discretized as co-located mesh by Finite Volume Method (FVM) and iteratively solved by Alternating Direction Implicit (ADI) scheme to obtain temperature and velocity field. The Pressure Weighted Interpolation Method (PWIM) is incorporated to avoid pressure oscillation and allow the use of co-located mesh for fluid flow, making the model computationally efficient. The model is validated for Ti6Al4V and Inconel 718 alloy with the experimental findings from the literature. The obtained results are in good agreement with an average deviation of 5.78% and 20.07% for Ti6Al4V , whereas for Inconel 718, 7.87 and 19.53% for melt-pool depth and width, respectively, were observed. Subsequently, the melt-pool growth and characteristics influenced by various process parameters are also studied.</p> <p><b>Graphical Abstract</b></p>  <p>The graphical abstract is divided into three main sections. The left section, titled 'LPBF Process', shows a 3D schematic of a laser powder bed fusion setup with labels for Laser Source, Nozzle, Powder Bed, and Build Platform. Below this is a diagram of 'Physical Phenomena Involved in the Process' showing laser energy input, powder bed, and melt pool. The middle section, titled 'Finite Volume grid cluster for 2D Domain', shows a 2D grid of triangular elements and a flowchart of the 'Algorithm' for solving the equations. The right section, titled 'Melt-Pool Temperature &amp; Velocity Distribution', shows a color-coded temperature map of the melt pool and a line graph of 'Results' showing temperature and velocity profiles.</p>
52.	<p><a href="#">Spatial concentration of Indian service industries in rural and urban areas: A micro-unit-level analysis</a>  <b>S Agarwal, SR Behera - Cogent Economics &amp; Finance, 2023</b></p> <p><b>Abstract</b>  This paper explores the spatial concentration of 120 service industries in India's rural and urban areas, covering 33.60 million establishments using Economic census (2013) data at the district level. Besides, this study uses a cartogram map to examine knowledge-intensive business services (KIBS) industries' spatial concentration patterns and geographical concentration of employment of workers in rural and urban areas in India. Empirical results show that the magnitude of the spatial concentration effect varies in rural and urban areas. Further, empirical results reveal that KIBS industries are localized in rural and urban areas but have a skewed distribution toward urban areas. Moreover, results show that hotspots in rural areas seem higher than urban hotspots, although rural hotspots employ fewer employees than urban hotspots. The empirical results suggest that urban planners and district municipal authorities can give more emphasis and implement suitable KIBS industry-specific policies to boost regional economic growth and employment in rural and urban India.</p>
53.	<p><a href="#">Spectroscopic performance evaluation and modeling of a low background HPGe detector using GEANT4</a>  <b>S Thakur, S Devi, SS Kaintura, K Tiwari, PP Singh - Nuclear Instruments and Methods in Physics Research, Section A: Accelerators, Spectrometers, Detectors and Associated Equipment, 2023</b></p> <p><b>Abstract</b>  Low background gamma spectrometry employing HPGe detectors is a sensitive technique for measuring low-level radioactivity in environmental applications, material screening, and for rare decay searches. This work presents spectroscopic performance evaluation and modeling of a low background measurement setup developed at IIT Ropar in Punjab, India, to measure trace natural radioactive elements, with a particular interest in studying low-level radioactivity in soil and/or</p>

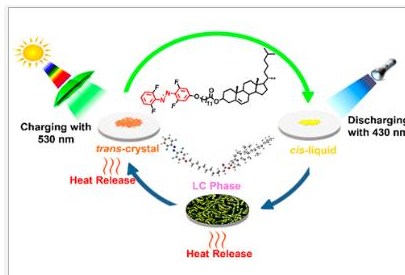
	<p>rock samples to generate specific inputs for low background experiments. The performance test and characterization of a low background cryocooled HPGe detector with relative efficiency of ~33% have been carried out. An effective detector model has been developed using GEANT4 Monte Carlo simulation to determine the response of the detector over an energy range of 80.9–1408 keV and compared with the experimental performance of the detector. The response of the detector obtained using Monte Carlo simulations agrees reasonably well within 93% level of confidence, indicating only 7% deviation in the comparison. The present setup offers improved detection limits of primordial radionuclides (U/Th and K) to measure radioactive contamination in environmental matrices, which has been used elsewhere (Thakur, 2023).</p>
54.	<p><a href="#">Synthesis of calix [4]arene-based nanohybrids: An efficient route for the electrochemical detection of dCO<sub>2</sub> and its sustainable transformation for the production of formic acid, a industrially valuable chemical</a> H Kaur, Divya, N Kaur, N Singh - Materials Today Sustainability, 2023</p> <p><b>Abstract</b> CO<sub>2</sub> exposure has damaging effects on human health and environment; therefore, its detection and sustainable capture and conversion has applications for both industrial and domestic use. <u>Electrochemical method</u> is a simple and reliable technique for selective quantification of dCO<sub>2</sub> and gCO<sub>2</sub>. Herein, we have developed electrochemical method for determination of dissolved CO<sub>2</sub> (dCO<sub>2</sub>) employing calix [4]Arene-based <u>nanohybrids</u> using NaHCO<sub>3</sub> as the carbon source exhibiting limit of detection (LOD) of 0.006 µM (<math>1.5 \times 10^{-6}</math> hPa CO<sub>2</sub>). The nanohybrids were produced by reducing Ag(I) on the surface of organic <u>nanoparticles</u> developed from calix [4]arene molecule. The calix [4]arene based dipodal receptor was synthesized using a <u>Schiff base condensation reaction</u> and organic nanoparticles were prepared by reprecipitation method. To reduce the carbon footprint, we have attempted to convert dCO<sub>2</sub> into formic acid (yield &gt;97%) electrochemically employing <u>AgNPs</u> nanohybrids as an efficient catalyst in slightly acidic medium and the conversion was characterized using NMR and FT-IR spectroscopy. The proposed method is highly efficient, simple and sustainable method to reduce CO<sub>2</sub> into formic acid and the practical utility of the proposed methodology was validated on bottled beverages (carbonated drinks), aquarium water, algae containing water, distilled water and fresh river water.</p>
55.	<p><a href="#">Tailoring the porosity and active sites in silicoaluminophosphate zeolites and their catalytic applications</a> JH Advani, A Kumar, R Srivastava - Catalysis in Confined Frameworks: Synthesis, Characterization, and Applications, 2023</p> <p><b>Abstract</b> Silicoaluminophosphate (SAPO) zeolites have emerged as attractive catalysts for various industrial applications due to their unique porosity and active sites. SAPOs are a family of crystalline microporous materials with customizable topologies and chemical compositions that make them appealing for various catalytic processes. This chapter provides insights into the porosity and active sites of SAPO zeolites and explores their catalytic applications in diverse chemical reactions, such as hydrocarbon conversion, selective oxidation, and acid-catalyzed processes. The fundamental characteristics of SAPOs and insights into the design and optimization of innovative SAPO-based catalysts with increased activity and selectivity would pave the path for developing new SAPO materials for their applications in petrochemical, fine chemicals, and renewable chemicals.</p>
56.	<p><a href="#">Take expert advice judiciously: combining groupwise calibrated model probabilities with expert predictions</a> S Gupta, S Jain, SS Jha... - Frontiers in Artificial Intelligence and Applications: Conference Paper, 2023</p> <p><b>Abstract</b> Training the machine learning (ML) models require a large amount of data, still the capacity of these models is limited. To enhance model performance, recent literature focuses on combining ML models' predictions with that of human experts, a setting popularly known as the human-in-the-loop or human-AI teams. Human experts can complement the ML models as they are well-</p>

	<p>equipped with vast real-world experience and sometimes have access to private information that may not be accessible while training the ML model. Existing approaches for combining an expert and ML model either require end-to-end training of the combined model or require expert annotations for every task. End-to-end training further needs a custom loss function and human annotations, which is cumbersome, results in slower convergence, and may adversely impact the ML model's accuracy. On the other hand, using expert annotations for every task is also cost-ineffective. We propose a novel technique that optimizes the cost of seeking the expert's advice while utilizing the ML model's predictions to improve accuracy. Our model considers two intrinsic parameters: the expert's cost for each prediction and the misclassification cost of the combined human-AI model. Further, we present the impact of group-wise calibration on the combined model that improves the overall model's performance. Experimental results on our combined model with group-wise calibration show a significant increase in accuracy with limited expert advice against different established ML models for the image classification task. In addition, the combined model's accuracy is always greater than that of the ML model, irrespective of the expert's accuracy, the expert's cost, and the misclassification cost.</p>
57.	<p><a href="#">Thermal performance evaluation of micro pin–fin heat exchangers: part i—geometrical design parameters optimization</a>  <b>H Kishore, M Pal, CK Nirala, A Agrawal</b> - International Journal of Precision ..., 2023</p> <p><b>Abstract</b>  In this work, evaluation of thermal losses formulated on the “Entropy Generation Minimization” (EGM) approach is performed to design arrayed micro pin–fin (MPF) heat sinks. The thermodynamic approach primarily evaluates the effects of different thermal parameters: thermal resistance, pressure drop, Nusselt number, etc. The objective function in the EGM is formulated using the search-based Particle swarm optimization (PSO) algorithm on MATLAB® to optimize the dimensional parameters of the MPFs. The characteristic length, height, inter-MPF gaps, cross-sectional area, perimeter, and density of the MPFs are considered decisive design parameters for geometrical Optimization in inline and staggered patterns. The PSO code has run for 1000 iterations at optimal operating parameters. Eventually, the staggered pattern of the arrayed heat sink showed a prospective reduction in design parametric values over the inline pattern for constant heat sink volume and thermal loading conditions. The optimal design parameters are used to model various unconventional cross-sectional profiles, viz. elliptical, aerofoil, droplet, and piranha, of MPFs for numerical simulations. The manufacturing feasibility of the optimized profile of the MPFs heat sink is explored and verified for near-net-shape fabrication using a popular and novel microfabrication technology, presented in Part II of the work.</p>
58.	<p><a href="#">Total cost of ownership analysis of fuel cell electric vehicles in India</a>  <b>UR Sontakke, S Jaju, DK Mahajan</b> - Towards Hydrogen Infrastructure: Advances and Challenges in Preparing for the Hydrogen Econom, 2023</p> <p><b>Abstract</b>  India is one of the largest importers of fossil fuels and at the same time one of the largest emitters of greenhouse gases by burning these imported fossil fuels. Therefore, self-reliance in the energy sector through clean energy is an immediate requirement. The transportation sector is one of the fastest-growing sources of carbon emission in India and thus replacing conventional internal combustion engine vehicles (ICEV) with electric powertrains vehicles based on batteries or fuel cells can provide an ultimate solution. The Government of India (GoI) under the recently launched Faster Adoption and Manufacturing of Electric Vehicles-II (FAME-II) scheme, is providing subsidies for battery electric vehicles (BEVs) amounting up to 40% of initial vehicle cost. BEVs, however, are not a true zero-emission solution due to the fossil fuel-dominated energy mix of India. In addition, BEVs have inherent limitations like limited travel range, long charging times, and extreme sensitivity to the high temperatures prevalent in India. Fuel cell</p>



	<p>electric vehicles (FCEVs), on the other hand, provide a true zero-emission alternative for the transportation sector. However, due to their high initial cost (and lack of hydrogen filling stations), FCEVs are not as popular as BEVs. For understanding the cost competitiveness of FCEVs in the Indian context, a total cost of ownership (TCO) analysis that includes not only their initial cost but also operational cost over the total life of the vehicle is required. To provide such insights, in this work TCO analysis of FCEVs is performed by considering the total life of the vehicle to be twelve years in comparison to BEVs and ICEVs. A realistic approach is adopted by considering the average annual distance traveled, the fuel cost, and average electrical energy consumption. The role of subsidy, as provided to BEVs under the FAME-II scheme, is also considered for evaluating the cost competitiveness of FCEVs in comparison to BEVs. © 2024 Elsevier Inc. All rights reserved.</p> <p><b>Author keywords</b>  Battery electric vehicles; Faster Adoption and Manufacturing of Electric Vehicles-II scheme; Fuel cell electric vehicles; Total cost of ownership</p>
59.	<p><a href="#">Viscous fingering instabilities in spontaneously formed blisters of MoS2 multilayers</a>  <b>M Pandey, R Ahuja, R Kumar</b> - <i>Nanoscale Advances</i>, 2023</p> <p><b>Abstract:</b>  The viscous fingering in the Hele-Shaw cell can be suppressed by replacing the upper-bounding rigid plate with an elastic membrane. Recently, graphene multilayers while polymer-curing-induced blistering showed the dynamical evolution of viscous fingering patterns on a viscoelastic substrate due to their thickness-dependent elasticity. Under certain conditions, the elastic solid-based instability couples with the viscoelastic substrate-based instability. The mechanisms underlying such a coupling in the blisters of 2D materials and the dynamical evolution of the viscous fingering patterns underneath the blisters are yet to be addressed. Herein, we investigate the viscous fingering instabilities in spontaneously formed blisters of MoS2 multilayers, and provide thorough analytical and experimental insights for the elucidation of the dynamical evolution of the viscous fingering patterns and the coupled instabilities in the blisters. We also estimate the interfacial adhesion energy of the MoS2 flakes over a (poly)vinyl alcohol (PVA) substrate and the confinement pressure inside the MoS2 blisters using a conventional blister-test model. It is observed that the presence of instability gives rise to anomalies in the modeling of the blister test. The adhesion mechanical insights would be beneficial for fundamental research as well as practical applications of 2D material blisters in flexible optoelectronics.</p> 
60.	<p><a href="#">Visible-light responsive azobenzene and cholesterol based liquid crystals as efficient solid-state solar-thermal fuels</a>  <b>AK KM, S Sony, S Dhingra, M Gupta</b> - <i>ACS Materials Letters</i>, 2023</p> <p><b>Abstract</b>  Solar-thermal fuels (STFs) based on photoresponsive molecules, which can harvest and store solar energy by the configurational change of molecules and can release it in the form of heat on demand, have been investigated recently. So far, azobenzene has been the most widely studied molecule for these applications. However, until now, only solid and liquid derivatives of azobenzene have been explored which suffer from several limitations. Here, we are reporting for the first time visible-light responsive STFs based on liquid crystals (LCs). We have prepared a series of compounds based on azobenzene and cholesterol with varying spacer and <i>ortho</i>-substitution on azobenzene. All of these derivatives exhibit enantiotropic chiral nematic (N*) mesophases. Moreover, they showed excellent photostability, photocyclability, and long half-life</p>

times of *cis*-states. We have further evaluated the thin films of these compounds for charging, i.e., *trans* to *cis* conversion under solar irradiation using various bandpass filters, and also studied the kinetics of the conversion. These compounds exhibited a maximum charging of up to 70% for the derivative with *ortho*-fluoro azobenzene. The charged thin films were further evaluated for their heat release properties by infrared (IR) thermal imaging. The maximum heat release observed was around 5.4 °C from the surrounding temperature which was significantly higher as compared to similarly substituted azobenzene-based derivative without a LC phase.



**Disclaimer:** This publication digest may not contain all the papers published. Library has compiled the publication data as per the alerts received from Scopus and Google Scholar for the affiliation “Indian Institute of Technology Ropar” for the month of November, 2023. The author(s) are requested to share their missing paper(s) details if any, for the inclusion in the next publication digest.